V International Conference on Computational Methods in Marine Engineering
MARINE 2013
B. Brinkmann and P. Wriggers (Eds)

NUMERICAL STUDY OF THE FLOW FIELD AROUND FISHING NET

YUN-PENG ZHAO[*], CHUN-WEI BI[*], GUO-HAI DONG[*], YU-CHENG LI[*] AND FU-KUN GUI[†]

[*] State Key Laboratory of Coastal and Offshore Engineering
Dalian University of Technology
Dalian 116024, China
e-mail: Zhaoyp18@hotmail.com

[†] Marine Science and Technology School
Zhejiang Ocean University
Zhoushan, 316000, China

Key words: Flexible Fishing Net, Flow Field, Porous Media Model, Lumped-mass Model

Abstract. A numerical approach is proposed to simulate the interaction between flow and fishing net in steady current. The numerical approach is based on the joint use of the porous media model and the lumped-mass model. The configuration of flexible net can be simulated using the lumped-mass model and the flow field around plane nets can be simulated using the porous media model. Using an appropriate iterative scheme, the fluid-structure coupling problem can be solved and the steady flow field around flexible net is available. In order to validate the numerical approach, the numerical results are compared with the data obtained from the physical model tests. The comparisons show that both the configuration of the flexible nets and flow velocity results are in accordance with that of the corresponding physical model tests.

1 INTRODUCTION

In a deep-water net cage, water motion is beneficial to maintaining the water quality and sufficient water exchange is important for the fish health and growth. However, too intense water motion can cause serious deformation of the fishing net and the effective volume of the net cage reduced sharply which is disadvantageous to fish comfort. Numerous studies have shown that, the force on cage net is proportional to the square of the flow velocity. Even if small velocity differences exist, this may lead to great force differences. So in the investigation on the forces acting on the net cage, the flow velocity distribution around the cage net usually cannot be ignored. Furthermore, the flow field characteristics determine the distribution of nutrients, refuse and dissolved oxygen in the net cage.

To our knowledge, the first investigation of the flow filed of net cages was performed by Aarsnes *et al*. [1]. A series of experiments were carried out to study the velocity distribution within net cage systems, and flow velocity reduction formulae for the net cages were developed. Over the decades since, much progress has been made in the understanding the flow filed inside and around net cages by experimental approach. Fredriksson [2] studied the flow velocity in an open ocean cage with field measurements, and an approximate 10% velocity reduction was found. Lader *et al*. [3] conducted a series of experiments to investigate

the forces and geometry of a net cage in uniform flow, and an average of 20% velocity reduction was measured inside the cage. Li *et al*. [4] analyzed the shadowing effect of six practical gravity cage models by physical model tests, and the flow reduction coefficients within and downstream of the net cages were obtained. Johansson *et al*. [5] performed field measurements at four farms in Norway, and major current reduction was measured in the current passing through the cages. The measured current reduction was between 33% and 64%. Harendza *et al*. [6] conducted experiments in a towing tank with particle image velocimetry (PIV) configurations to investigate the flow field around cylinder fish cages with varying inclination angles and porosity, and the effects of inclination and porosity were described.

However, the efforts mentioned above are mainly concentrated on physical model tests. The numerical study of the flow field around net structure is complex due to the innumerable meshes and other properties like flexibility and discontinuity. Patursson *et al*. [7] developed a numercial model to simulate the flow field around a plane net without considering the net deformation by treating the net structure as a porous medium. Zhao *et al*. [8] proposed a three-dimensional numerical model using the porous media model and presented the flow field inside and around multiple net cages. Through the review of literature on numerical works, the existing efforts are mainly concentrated on the flow field around net structure with no deformation, and there are few numerical models considering the flexibility and movement of the fishing net. This paper introduces a three-dimensional numerical approach to simulate the interaction between flow and flexible nets in a steady current.

2 MODEL DESCRIPTIONS

The numerical approach to simulate the interaction between flow and the flexible net includes two numerical models: the porous media model and the lumped-mass model. The porous media model can simulate the flow field around the plane net with no deformation, and the lumped-mass model can simulate the configuration of flexible nets in certain current. The joint use of the above two models is presented to solve the fluid-structure coupling problem. The steady flow field around flexible nets can be obtained by using an appropriate iterative scheme as explained later in Section 2.3.

2.1 The porous media model

In this part, the porous media model is introduced to model the flow field around the plane net with no deformation, and the finite volume method is used to solve the governing equations of the numerical model. In this way, the numerical simulation of the flow field around the plane net is available.

2.1.1 Porous media resistance coefficients

The porous media model employs empirically determined flow resistance in the region of the domain that is occupied by the porous media. For flow through the porous media, the hydrodynamic forces acting on the porous media can be expressed as follows:

$$F = S_i \lambda A \tag{1}$$

where S_i is the source term for the momentum equation in the i direction, λ is the thickness of the porous media, A is the area of the porous media, and F is the hydrodynamic force in the i direction.

In Eq.(1), S_i is the source term for the momentum equation. When the region is outside the porous media model, $S_i = 0$. While, inside the porous media, S_i is calculated by the following equation:

$$S_i = -\left(D_{ij}\mu u + C_{ij}\frac{1}{2}\rho|u|u \right);$$
$$D_{ij} = \begin{pmatrix} D_n & 0 & 0 \\ 0 & D_t & 0 \\ 0 & 0 & D_t \end{pmatrix}, C_{ij} = \begin{pmatrix} C_n & 0 & 0 \\ 0 & C_t & 0 \\ 0 & 0 & C_t \end{pmatrix}. \quad (2)$$

where D_{ij} and C_{ij} are prescribed material matrices consisting of the porous media resistance coefficients, D_n is the normal viscous resistance coefficient, D_t is the tangential viscous resistance coefficient, C_n is the normal inertial resistance coefficient, C_t is the tangential inertial resistance coefficient.

Substituting Eq. (2) into Eq. (1) provides formulas for calculating the drag force (F_d) and the lift force (F_l) of the plane net. The drag force is parallel to the flow direction, and the lift force is perpendicular to the flow direction:

$$F_d = \left(D_n\mu u + C_n\frac{1}{2}\rho|u|u \right)\lambda A \quad (3)$$

$$F_l = \left(D_t\mu u + C_t\frac{1}{2}\rho|u|u \right)\lambda A \quad (4)$$

The porous coefficients in Eqs. (3) and (4) can be calculated from the drag and lift forces, while the drag and lift forces acting on the fish net have strong relationship with the features of fish net. So the connection between net features and flow field is considered by the porous coefficients in our numerical model. In a general way, the drag and lift forces of the plane net are obtained from the laboratory experiments. In addition, the forces can be calculated from the Morison equation:

$$F_d = \frac{1}{2}\rho C_d A u^2 \quad (5)$$

$$F_l = \frac{1}{2}\rho C_l A u^2 \quad (6)$$

where C_d and C_l are coefficients that can be calculated using empirical formulas proposed by Zhan *et al*. [9], Løland [10], Aarsnes *et al*. [1], etc.

When the plane net is oriented normal to the flow, the porous coefficients (D_n and C_n) are chosen from a curve fit between drag force data of the plane net and corresponding current velocities using the least squares method. The other two coefficients (D_t and C_t) can be ignored because the lift force is equal to 0 when α=90°. When the plane net is oriented with different attack angles (see Figure 1), the porous coefficients should be transformed into formulas (7) and (8) [11]. Then, the four porous coefficients can be obtained by minimizing the error between the theoretical values and existing data for the drag and lift forces using the least squares method, which is a common analytical method in error minimization.

$$D_n^{'} = \frac{D_n + D_t}{2} + \frac{D_n - D_t}{2}\cos(2\alpha^{'})$$
$$C_n^{'} = \frac{C_n + C_t}{2} + \frac{C_n - C_t}{2}\cos(2\alpha^{'}) \quad (7)$$

$$D_t^{'} = \frac{D_n - D_t}{2}\sin(2\alpha^{'})$$
$$C_t^{'} = \frac{C_n - C_t}{2}\sin(2\alpha^{'}) \quad (8)$$

where $\alpha^{'} = 90^{o} - \alpha$, and α is the attack angle.

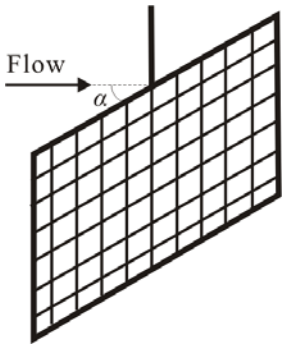

Figure 1: Definition of attack angle (α). Note that the attack angle describes the angle between the flow direction and the plane net in the horizontal plane.

2.1.2 Mesh grids and boundary conditions

An example of computational grids of a plane net at an attack angle α=90° is shown in Figure 2. The optimal mesh type and grid size can be achieved by using the tetrahedron mesh and a size fuction. The coordinate system for the numerical model is a right-handed, three-dimensional Cartesian coordinate system. The origin of the coordinate system is set to the center of the plane net on the free surface. In the coordinate system, x is positive along the flow direction, y is perpendicular to the flow direction on the horizontal plane and z is negative along the direction of the acceleration of gravity. The left boundary of the numerical flume is described by the velocity-inlet boundary condition, while the right boundary is described by the outflow boundary condition. The free surface is modeled using the wall boundary condition with zero shear force. The solid surfaces are modeled using no slip wall boundary. In the areas close to the solid surfaces, the technique of wall function and boundary layer mesh are adopted to solve the effect of the wall surfaces.

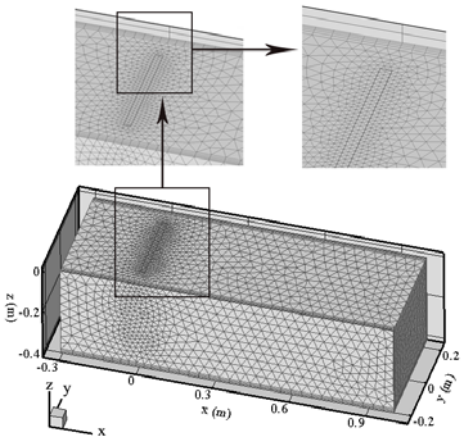

Figure 2: Example of the computational grids.

2.2 The lumped-mass model

The lumped-mass model is introduced to simplify the flexible net (see Figure 3), and the motion equation can be established mainly based on Newton's second law. Given an initial net configuration, the motion equations can be solved numerically for each lumped-mass point. Finally, the configuration of the flexible net in current can be simulated. The calculation method for the model has been explained fully in our previous articles [12,13]. Here only a brief outline is described.

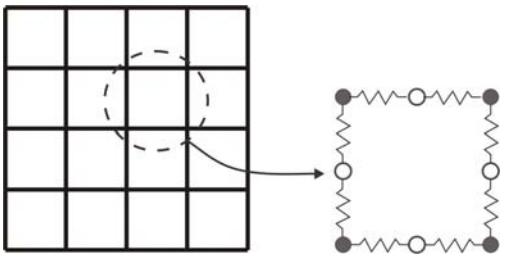

Figure 3: Sketch of the lumped-mass model.

2.2.1 Hydrodynamic forces and motion equations

In a uniform current, the motion equation of lumped-mass i can be expressed as follows:

$$(M_i + \Delta M_i)\vec{a} = \sum_{j=1}^{n} \vec{T}_{ij} + \vec{F}_d + \vec{B} + \vec{W}$$
$$\Delta M = \rho \forall C_m^{'}, C_m = 1 + C_m^{'} \tag{9}$$

where M_i and ΔM_i are the mass and added-mass of lumped-mass point i, $\forall$ is the volume of the point, C_m is the inertial force coefficient, $C_m^{'}$ is the added-mass coefficient, $\vec{a}$ is the acceleration of mass point, $\vec{T}_{ij}$ is the tension force in twine ij (j is the code for knots at another

end of the bar *ij*), *n* is the number of adjacent knots of point *i*, $\vec{F}_d$,$\vec{W}$ and $\vec{B}$ are the drag force, gravity force and buoyancy force, respectively.

Since the points at mesh bars are assumed to be cylindrical elements, the direction of the fluid forces acting on the point masses at each mesh bar should be considered. Therefore, the motion of the point mass *i* is set at the center of a mesh bar, and a local coordinates (τ, η, ξ) are defined to simplify the procedure (see Figure 4). The origin of the local coordinate is set at the center of a mesh bar and the η-axis lies on the plane including τ-axis and flow velocity $\vec{V}$.

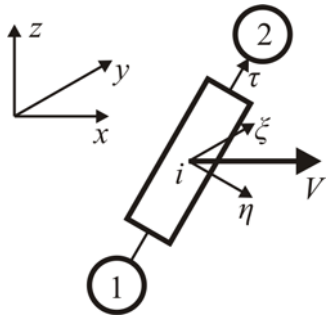

Figure 4: Sketch of the local coordinate for a mesh twine.

Besides the gravity and buoyancy, the drag force on lumped-mass point can be obtained by Morison Equation as follows:

$$\begin{aligned} F_{D\tau} &= -\frac{1}{2}\rho C_{D\tau} A_\tau \left|\vec{V}_\tau - \vec{\dot{R}}_\tau\right| (\vec{V}_\tau - \vec{\dot{R}}_\tau) \\ F_{D\eta} &= -\frac{1}{2}\rho C_{D\eta} A_\eta \left|\vec{V}_\eta - \vec{\dot{R}}_\eta\right| (\vec{V}_\eta - \vec{\dot{R}}_\eta) \\ F_{D\xi} &= -\frac{1}{2}\rho C_{D\xi} A_\xi \left|\vec{V}_\xi - \vec{\dot{R}}_\xi\right| (\vec{V}_\xi - \vec{\dot{R}}_\xi) \end{aligned} \tag{11}$$

where ρ is the density of water, $C_{D\tau}$, $C_{D\eta}$ and $C_{D\xi}$ are the drag coefficient in their respective directions, A_τ, A_η and A_ξ are the projected area of twine normal to their respective directions, $\vec{\dot{R}}_\tau$, $\vec{\dot{R}}_\eta$, $\vec{\dot{R}}_\xi$, $\vec{V}_\tau$, $\vec{V}_\eta$ and $\vec{V}_\xi$ are the velocity components of the lumped-mass point and water particle in their respective directions. The drag coefficients related to Reynolds number are described in the section 2.2.2.

The configuration of the fishing net in current at each time step can be calculated numerically by solving the motion equation with a given initial condition. The equations are simultaneously solved by using the Runge-Kutta-Verner sixth-order method in this paper. The tolerance for the global error is set to 0.001 to guarantee calculation accuracy. In all simulations, the time step is set to 0.001 and the simulation time is set to 40 s considering the calculation precision and efficiency.

2.2.2 Hydrodynamic coefficients of the net

For each mesh bar, the numerical procedure calculates the drag coefficient C_η and C_τ using a method described by Choo and Casarella [14] that updates the drag coefficients based on the Reynolds number (Re_n) as follows:

$$C_\eta = \begin{cases} \dfrac{8\pi}{\mathrm{Re}_n s}\left(1-0.87s^{-2}\right) & \left(0<\mathrm{Re}_n\le 1\right) \\ 1.45+8.55\,\mathrm{Re}_n^{-0.90} & \left(1<\mathrm{Re}_n\le 30\right) \\ 1.1+4\,\mathrm{Re}_n^{-0.50} & \left(30<\mathrm{Re}_n\le 10^5\right) \end{cases} \tag{12}$$

$$C_\tau = \pi\mu(0.55\,\mathrm{Re}_n^{1/2}+0.084\,\mathrm{Re}_n^{2/3}) \tag{13}$$

where $\mathrm{Re}_n = \rho V_{Rn} D/\mu$, $s = -0.077215665 + \ln(8/\mathrm{Re}_n)$, μ is the viscosity of water, C_η and C_τ are the normal and tangential drag coefficients for mesh bar, V_{Rn} is the normal component of the fluid velocity relative to the bar, and ρ is the density of water.

For the knot part, the Fredheim and Faltinsen [15] suggested it could be reasonable to use a drag coefficient in the range of 1.0–2.0 when modeling the knot part as a sphere. Here C_D is set as 2.0 for the knot part.

2.3 Joint use of the porous media model and the lumped-mass model

The lumped-mass model is introduced to simplify the flexible net, and the motion equation can be established The main concept of the numerical approach is to combine the porous media model and the lumped-mass model to simulate the interaction between flow and flexible nets. Taking single flexible net as example, a calculating flow chart for the numerical approach is shown in Figure 5. More detailed calculation procedure is given as follows. Step 1 is to simulate the flow field around a plane net without considering the net deformation using the porous media model. Step 2 is to calculate the drag force and the configuration of a flexible net in current using the lumped-mass model. The given initial flow velocity is exported from the upstream surface of the plane net in Step 1. In Step 3, according to the net configuration, the flow field around the flexible net can be simulated by dividing the net into several plane nets with different inclination angles. In Step 4, the drag force and the configuration of the flexible net is calculated again. Along the net height, different flow velocities are given which are exported from the upstream surface of the plane nets with different inclination angles. The terminal criterion of the calculation procedure is defined as $\Delta F = \left(F_{i+1} - F_i\right)/F_{i+1}$, where F_i and F_{i+1} are the drag forces of two adjacent calculations. If $\Delta F < 0.001$, it was determined that the force acting on the net structure is stable and the configuration of the flexible net is the equilibrium position considering the fluid-structure interaction. Otherwise, repeat Steps 3 and 4 until the criterion meets the precision requirement. Finally, the fluid-structure coupling problem can be solved and the steady flow field around flexible nets is available.

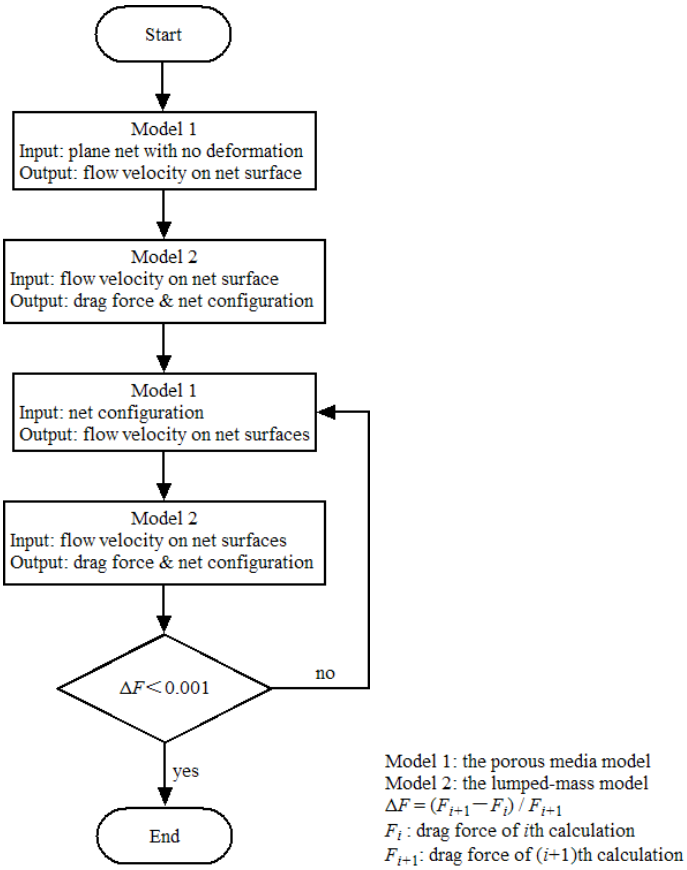

Figure 5: Flow chart for joint use of the porous media model and the lumped-mass model.

3 NUMERICAL SIMULATIONS OF THE INTERACTION BETWEEN FLOW AND FLEXIBLE NET

3.1 Laboratory setup

The tested net was a 0.3 m×0.3 m knotless polyethylene (PE) net with 15 meshes in width and 15 meshes in height. The twine diameter was 2.6 mm, and the mesh bar length was 20 mm. Mounted as square meshes, the net solidity ratio was 0.26. The flexible net, positioned from the water surface down, was centered on the width of the flume. A steel lower bar was mounted on the bottom of the net as sinker system. The diameter of the lower bar is 6 mm, and the mass is 73 g. Configuration of the flexible net was recorded using a CCD (Charge Coupled Device) camera at four different flow velocities, u_0=0.058, 0.113, 0.170 and 0.226 m/s. A load cell was attached to the top of the steel frame to measure the drag force on the flexible net. Meanwhile, flow velocities at three measurement points (see Figure 6) downstream from the flexible net were measured using an acoustic Doppler velocimeter (ADV).

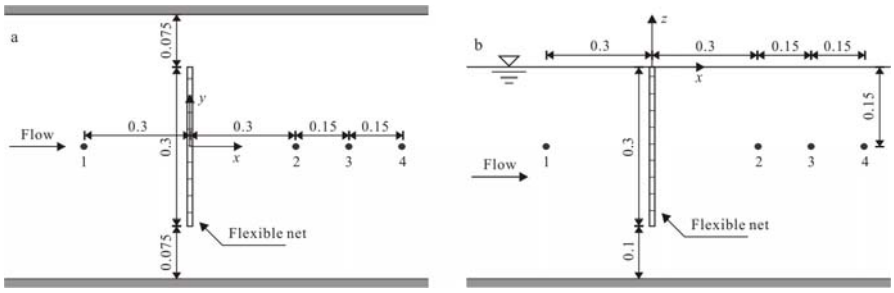

Figure 6: Physical model of a plane net and general setting of the measurement points (unit: m): (a) horizontal view and (b) vertical view.

3.2 Numerical model description

The three-dimensional numerical model was established according to the physical model. The characteristics of the fishing net are the same as in the physical model tests. The thickness of the porous media is 20 mm, and the porous coefficients, D_n=870,000 m^{-2}, D_t=153,500 m^{-2}, C_n=20.5 m^{-1}, and C_t=10.0 m^{-1}, can be obtained from the experimental data. The flexible net model is located 0.3 m downstream from the velocity-inlet boundary. The numerical simulations are performed with the incoming velocity u_0=0.226 m/s and u_0=0.170 m/s.

3.3 Results and discussion

The calculation precision and the equilibrium configuration of the flexible net can be obtained after the first iteration of Steps 3 and 4 in the numerical approach. In addition, the comparison of the equilibrium configuration of single flexible net between numerical simulation and physical model test presents a satisfactory result (see Figure 7).

The steady flow field around the flexible net is available according to the net configuration by dividing the net into several plane nets with different inclination angles. In the numerical results (see Figure 8), the streamlines present the flow direction around the flexible net. It was determined that the flow direction has no obvious diversion around the flexible net. That may be because the porosity of the net is quite large. As shown in the contour plots, there is a small region of flow velocity reduction upstream of the net, while there is a rather large velocity reduction region downstream from the net. As flow direction has no obvious diversion around the flexible net, the current reduction downstream from the net is mainly due to the shielding effect of the net. The width of the wake behind the net becomes narrower toward the centerline with increasing distance from the flexible net. The flow velocity increases at the flanks of the wake.

Comparisons of the flow velocity component u show that the flow velocity magnitude of the numerical simulation agrees well with the experimental data, and the maximum relative error is 1.9% (see Figure 9). Obvious flow velocity reduction of component u exists along the line through the net in the x direction. The maximum velocity reductions downstream from the single flexible net are 12.8% when u_0=0.226 m/s and 12.4% when u_0=0.170 m/s respectively according to our numerical results.

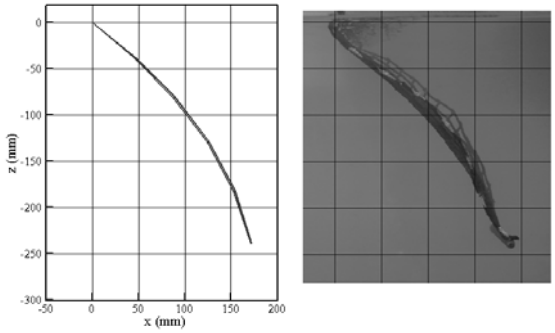

Figure 7: Comparison of the deformation of single flexible net between numerical simulation and physical model test when incoming velocity is 0.226 m/s.

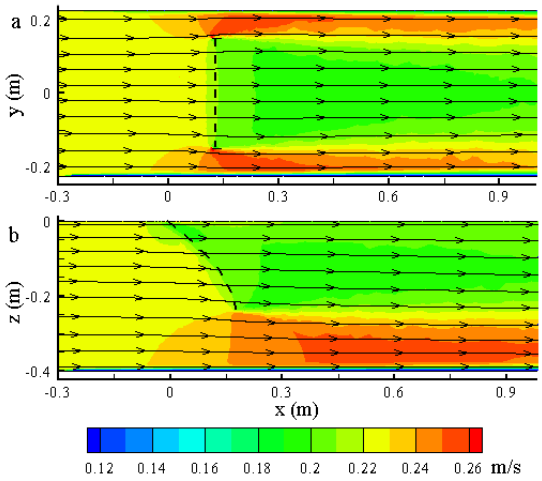

Figure 8: Flow velocity distribution around single flexible net calculated by numerical simulation when incoming velocity is 0.226 m/s: (a) contours on the horizontal plane z =−0.15 m and (b) contours on the vertical plane y =0.

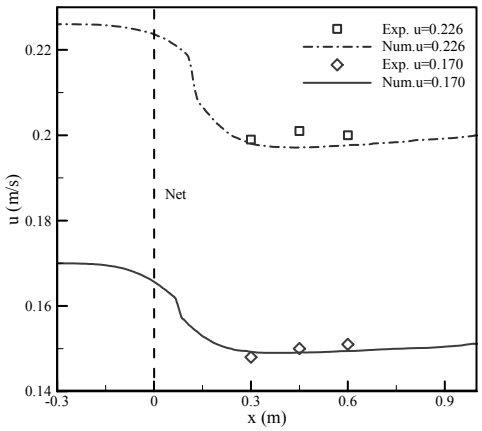

Figure 9: Comparisons of the flow velocity component u between numerical simulations and experimental data downstream from single flexible net.

4 CONCLUSIONS

- A numerical approach is proposed to simulate the interaction between flow and flexible nets based on the joint use of the porous media model and the lumped-mass model. Using an appropriate iterative scheme, the fluid-structure coupling problem can be solved and the steady flow field around flexible nets is available. The numerical results of the flexible net agree well with the experimental data. This study indicates that present numerical approach can simulate the interaction between flow and flexible net accurately.
- According to our numerical results, the diversion of flow direction around the flexible nets is relatively small. The maximum flow velocity reductions downstream from the single net are 12.8% and 12.4% respectively in two different currents.
- Present numerical approach is applicable to multiple flexible nets, and the number of iterations will not increase obviously. The incoming velocity is considered as the dominant factor for increasing the number of iterations.

ACKNOWLEDGEMENTS

This work was financially supported by the National Natural Science Foundation (NSFC) Project Nos.51239002, 51221961 and 51109187, the National 863 High Technology Project No.2006AA100301.

REFERENCES

[1] Aarsnes, J.V., Rudi, H. and Løland, G. Current forces on cage, net deflection. *In: Engineering for Offshore Fish Farming*. Thomas Telford, London, (1990) pp. 137–152.

[2] Fredriksson, D.W. *Open ocean fish cage and mooring system dynamics*. Ph.D. Dissertation, University of New Hampshire, Durham, NH, USA (2001).

[3] Lader, P.F., Enerhaug, B., Fredheim, A. and Krokstad, J. Modelling of 3D net structures exposed to wave and current. *In: 3rd International Conference on Hydroelasticity in Marine Technology* (2003) pp. 19-26.

[4] Li, Y.C., Chen, C.P., Li, C.L. and Mao, Y.C. A study on effectiveness of flow reducing by the net of gravity cage group. *Shipbuilding of China* (2005) **46**: 105-109. (in Chinese)

[5] Johansson, D., Juell, J.E., Oppedal, F., Stiansen, J.E. and Ruohonen, K. The influence of the pycnocline and cage resistance on current flow, oxygen flux and swimming behaviour of Atlantic salmon (Salmo salar L) in production cages. *Aquaculture*. (2007) **265**: 271-287.

[6] Harendza, A., Visscher, J., Gansel, L., Pettersen, B. PIV on inclined cylinder shaped fish cages in a current and the resulting flow field. *In: 27th International Conference on Offshore Mechanics and Arctic Engineering*, Estoril, Portugal, (2008) OMAE2008-57748.

[7] Patursson, Ø., Swift, M.R., Tsukrov, I., Simonsen, K., Baldwin, K., Fredriksson, D.W., Celikkol, B. Development of a porous media model with application to flow through and around a plane net. *Ocean Engineering* (2010) **37**: 314-324.

[8] Zhao, Y.P., Bi, C.W., Dong, G.H., Gui, F.K., Cui, Y., Xu, T.J. Numerical simulation of the flow field inside and around gravity cages. *Aquacultural Engineering* (2013) **52**: 1-13.

[9] Zhan, J.M., Jia, X.P., Li, Y.S., Sun, M.G., Guo, G.X. and Hu, Y.Z. Analytical and experimental investigation of drag on nets of fish cages. *Aquacultural Engineering* (2006) **35**: 91-101.

[10] Løland, G. *Current force on flow through fish farms*. Ph.D. Dissertation, Norwegian Institute of Technology, Trondheim, Norway (1991).

[11] Bear, J. *Dynamics of Fluids in Porous Media*. America Elsevier Publishing Company, Inc., New York (1972).

[12] Li, Y.C., Zhao, Y.P., Gui, F.K. and Teng, B. Numerical simulation of the hydrodynamic behaviour of submerged plane nets in current. *Ocean Engineering* (2006) **33**: 2352-2368.

[13] Zhao, Y.P., Li, Y.C., Gui, F.K. and Dong, G.H. Numerical simulation of the effects of weight system on the hydrodynamic behavior of 3-D net of gravity cage in current. *Journal of Hydrodynamics, Ser. B* (2007) **19**: 442-452.

[14] Choo, Y.I. and Casarella, M.J. Hydrodynamic resistance of towed cables. *Journal of Hydronautics* (1971) pp. 126–131.

[15] Fredheim, A. and Faltinsen, O.M. Hydroelastic anslysis of a Fishing net in steady inflow conditions. *In: Proceeding of 3rd International Conference on Hydroelasticity in Marine Technology*. University of Oxford, Oxford, Great Britain (2003).